Journal of Solid State Chemistry 183 (2010) 2528–2533

Contents lists available at ScienceDirect

Journal of Solid State Chemistry

journal homepage: www.elsevier.com/locate/jssc

A new phase in the system lithium–aluminum: Characterization of orthorhombic Li_2Al

Kati Puhakainen [a], Magnus Boström [b], Thomas L. Groy [a], Ulrich Häussermann [a,*]

[a] Department of Chemistry and Biochemistry, Arizona State University, Tempe, Arizona 85287-1604, USA
[b] Sandvik Materials Technology, S-881 81 Sandviken, Sweden

ARTICLE INFO

Article history:
Received 7 June 2010
Received in revised form
16 August 2010
Accepted 22 August 2010
Available online 26 August 2010

Keywords:
Lithium
Aluminum
Phase diagram

ABSTRACT

Investigation of the Li rich part of the binary Li–Al system revealed the existence of a new phase, orthorhombic Li_2Al, which is isostructural to Li_2Ga and Li_2In. The crystal structure was determined from single crystal X-ray diffraction data (*Cmcm*, $a=4.658(2)$ Å, $b=9.767(4)$ Å, $c=4.490(2)$ Å, $Z=4$). Refinement of atomic position site occupancies yielded a composition $Li_{1.92}Al_{1.08}$ (64 at% Li) indicating a small homogeneity range, $Li_{2-x}Al_{1+x}$. Li_2Al is the peritectic decomposition product of the stoichiometric compound Li_9Al_4, which is stable below 270 ± 2 °C. Li_2Al itself decomposes peritectically to Li_3Al_2 and Li rich melt at 335 ± 2 °C. The discovery of Li_2Al ($Li_{2-x}Al_{1+x}$) settles a long standing inconsistency in the Li–Al phase diagram which was based on the assumption that Li_9Al_4 possesses a high temperature modification.

1. Introduction

Interest in multinary high-strength low-density alloys and high capacity electrodes for Li batteries has fueled numerous investigations of the binary Li–Al system [1–6]. Most recently Hallstedt and Kim [7] provided a detailed review in the course of a Calphad type evaluation of available experimental data. The Li–Al system contains three stable phases. The β phase (LiAl) has a considerable, temperature dependent, homogeneity range and crystallizes in the NaTl structure [8]. Its maximum solubility ranges from about 48 to 55 at% Li. Li_3Al_2 is reported as "narrow phase" with a small, or zero, homogeneity range [6]. This phase crystallizes with a rhombohedral structure (Li_3Al_2 type) [9] which is also found for the heavier congeners Li_3Ga_2 [10] and Li_3In_2 [11]. Li_9Al_4 represents a stoichiometric line compound with a peculiar and unique monoclinic structure [12]. The Li rich phases decompose peritectically whereas the β-phase melts congruently at around 700 °C.

There are some apparent inconsistencies for the Li rich part of the Li–Al phase diagram. Thermal events have been reported at around 267 or 242 °C [2,3] and interpreted as the transformation of monoclinic Li_9Al_4 into a high temperature phase [6]. However, the characterization of such a phase has never been undertaken. In this paper we report on the synthesis and structural characterization of a new phase in the Li–Al system, Li_2Al. The discovery of this phase explains the previously reported thermal events and rules out the existence of a high temperature phase for Li_9Al_4.

2. Experimental section

2.1. Synthesis and phase characterization

All steps of synthesis and sample preparation were performed in an Ar-filled glovebox (H_2O and O_2 concentrations <0.3 ppm). Starting materials were rods of Li (99.9%) and pellets of Al (99.99+, 3–8 mesh) purchased from Sigma-Aldrich.

Mixtures with the compositions $Li_{91.5}Al_{8.5}$ and $Li_{96}Al_4$ and total masses of about 1 g were loaded into specially prepared Ta ampoules. The chosen compositions targeted an equilibrium between melt and Li richest phase at a certain temperature. The melt will then be separated from the solid phase by isothermal centrifugation which should allow access to well crystallized samples of Li_9Al_4 and its high temperature modification (provided the latter exists and is metastable). The method of isothermal "melt-centrifugation" has been successfully applied for studying the Ga rich portion of various transition metal–Ga systems [13]. For these investigations reaction mixtures were enclosed in silica ampoules. However, with alkali metals involved, metal ampoules have to be employed.

A sketch of the here employed metal ampoule is shown in Fig. 1. It consisted of a piece of seamless Ta tubing (length 75, ID=9, OD=10 mm) with a filter inserted and round lids welded on the top and bottom. Filter and lids were fabricated from a Ta sheet (0.5 mm thickness) by punching out disks and forming them cup shaped. For becoming filters, cups were perforated by small

* Corresponding author.
E-mail address: Ulrich.Haussermann@asu.edu (U. Häussermann).

0022-4596/$ - see front matter © 2010 Elsevier Inc. All rights reserved.
doi:10.1016/j.jssc.2010.08.029

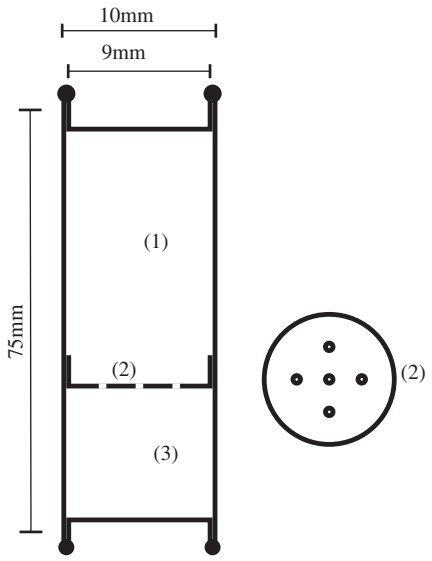

Fig. 1. Sketch of the Ta reaction container used for isothermal "melt-centrifugation" synthesis: (1) indicates the sample space, (2) the filter and (3) the centrifugate space.

hole electrical discharge machining (EDM) drilling (0.5 mm hole sizes).

When preparing for a synthesis run, first the filter was inserted in the Ta tube and the lid that closes the centrifugate space was welded. Then the reaction mixture was loaded and the lid closing the sample space welded. Subsequently the Ta ampoule was brought outside the glove box and sealed in a silica jacket. The silica jacket was placed – with the sample space at the bottom – in a silica wool insulated reaction container made of stainless steel. The container was subsequently placed into a box furnace. The reaction mixture was heated to 450 °C at a rate of 300 °C/h, kept at this temperature for 1 h, and then cooled at a rate of 5 °C/h to 300 °C ($Li_{91.5}Al_{8.5}$) or to 210 °C ($Li_{96}Al_4$). The mixtures were left at their target temperatures for 7 days. Thereafter, the stainless steel container was turned upside down (centrifugate space at the bottom) and rapidly inserted into a centrifuge which was operated at 3000 rpm for 3 min. The Ta ampoules were opened inside the glove box at the end of the sample space. The crystalline product that collected on the filter was released by gently squeezing the waist of the Ta tube with a pair of pliers.

The highly moisture sensitive products were analyzed by powder X-ray diffraction. Samples were ground and loaded into 0.3 mm capillaries. Measurements were performed on a Bruker D8 Advance diffractometer (Göbel mirror, Cu$K\alpha$ radiation) for a 2θ range from 10° to 90° with an increment step of 0.014°.

2.2. Thermal analysis

A pelletized sample of 10–15 mg was hermetically sealed under argon atmosphere in a TA Tzero® aluminum pan. Differential scanning calorimetry (DSC) was performed using a Mettler-Toledo TGA/DSC 1 instrument. A nitrogen gas flow of ~0.04 l/min was applied. Scanning ranges were from 50 to 300 °C and from 50 to 380 °C. The heating/cooling rate was 10 °C/min. At the maximum temperature the sample was equilibrated for 5 min. Temperature and heat flow were calibrated using indium (T_m=156.6 °C, ΔH_{fus}=28.5 J/g) and tin (T_m=231.9 °C, ΔH_{fus}=59.2 J/g). Data acquisition and evaluation were performed with the Mettler STAR^e v.9.30 software. For integration a horizontal baseline was applied.

2.3. Crystal structure characterization

Regularly shaped single crystals suitable for intensity data collection were obtained by crushing larger product specimens between two glass slides. Crystals were sealed in 0.3 mm capillaries. Intensity data was collected at room temperature on a SMART APEX system using graphite monochromated Mo$K\alpha$ radiation (λ=0.71073 Å) and corrected for Lorentz and polarization effects. Absorption correction was performed by the program SADABS [14]. Space groups were assigned on the basis of the systematic absences and the statistical analysis of the intensity distributions. Structure determination (direct methods) and refinement (full-matrix least squares on F^2) was performed with the programs SHELXS-97 and SHELXL-97, respectively [15]. Some details of the single crystal data collections and refinements are listed in Table 1. Atom position parameters and selected interatomic distances are given in Tables 2 and 3. Further details of the crystal structure investigations may be obtained as supporting information and from Fachinformationszentrum Karlsruhe, D-76344 Eggenstein-Leopoldshafen, Germany (fax: (+49)7247-808-666; e-mail: crysdata@fiz-karlsruhe.de) on quoting the depository nos. CSD-421853 (Li_2Al) and CSD-421854 (Li_9Al_4)).

3. Results and discussion

3.1. The lithium rich side of the Li–Al system

Fig. 2a shows the Li rich part of the Li–Al phase diagram according to McAllister [6]. It includes an isotherm at 275 °C that indicates a high temperature (HT) phase transition of Li_9Al_4. The

Table 1
Summary of crystallographic data and structural analysis for Li_2Al and Li_9Al_4.

Analysis for	Li_2Al	Li_9Al_4
Formula	$Li_{1.92(1)}Al_{1.08(1)}$	Li_9Al_4
Formula weight	42.5	170.38
Crystal size, mm^3	0.13 × 0.11 × 0.10	0.37 × 0.25 × 0.14
Space group	*Cmcm* (No. 63)	*C*2/*m* (No. 12)
a, Å	4.6579(16)	18.916(4)
b, Å	9.767(4)	4.5041(11)
c, Å	4.4901(16)	5.4249(14)
β, deg	90.00	105.19(3)
Z; *V*, Å^3	4; 204.28(12)	2; 446.05(20)
D_{calc}, g cm^{-3}	1.381	1.269
Temp, K	298(2)	298(2)
λ(Mo$K\alpha$), Å	0.71073	0.71073
Absorption coeff., mm^{-1}	0.493	0.420
F(000)	79	158
θ_{min}–θ_{max}, deg	4.174–32.972	2.23–24.85
Index ranges	$-6<h<6$, $-12<k<12$, $-5<l<5$	$-6<h<22$, $-5<k<5$, $-6<l<6$
Total reflns collected	500	5681
Independent reflns	145[*R*(int)=0.0425]	452 [*R*(int)=0.0197]
Refinement method	full-matrix least-squares on F^2	full-matrix least-squares on F^2
Data/restraints/params	145/0/15	452/0/41
Final *R* indices [$I>3\sigma(I)$][a,b]	*R*1=0.0251, wR_2=0.0545	*R*1=0.0170, wR_2=0.0413
R indices (all data)[a,b]	*R*1=0.0286, wR_2=0.0558	*R*1=0.0181, wR_2=0.0419
Largest diff. peak and hole, e$^-$Å^{-3}	0.183 and −0.183	0.129 and −0.160
GOF on F^2	1.056	1.120

[a] $(R_1)=\sum||F_o|-|F_c||/\sum|F_o||$.
[b] $wR_2=\{\sum[w(F_o^2-F_c^2)^2]/\sum[w(F_o^2)^2]\}^{1/2}$.

Table 2
Fractional atomic coordinates and equivalent atomic displacement parameter for Li_2Al and Li_9Al_4 with estimated standard deviations in parentheses.

	Atom	Wyck.	Occ.	*x*	*y*	*z*	U_{iso} (Å^2)
Li_2Al	Al	4*c*	1	0	0.07477(9)	1/4	0.0186(3)
	Li1	4*c*	0.95	0	0.7582(5)	1/4	0.034(2)
	Al1	4*c*	0.048(5)				
	Li2	4*c*	0.96	1/2	0.4093(5)	1/4	0.033(2)
	Al2	4*c*	0.036(6)				
Li_9Al_4	Al1	4*i*	1	0.15030(2)	0	0.21378(6)	0.0158 (1)
	Al2	4i	1	0.38538(1)	0	0.06429(5)	0.0166(1)
	Li1	2*a*	1	0	0	0	0.0263(7)
	Li2	4*i*	1	0.0856(1)	0	0.3590(4)	0.0186(4)
	Li3	4*i*	1	0.2330(1)	0	0.8431(4)	0.0301(6)
	Li4	4*i*	1	0.3081(1)	0	0.4765(4)	0.0215(5)
	Li5	4*i*	1	0.4566(1)	0	0.6745(4)	0.0266(5)

Table 3
Interatomic distances below 3.5 Å for Li_2Al and Li_9Al_4. Standard deviations are given in parentheses.

Atom pair	Li_2Al	Atom pair	Li_9Al_4	Atom pair	Li_9Al_4
Al–Al × 2	2.678(1)	Al1–Al2 × 2	2.6962(6)	Al2–Al1 × 2	2.6962(6)
–Li1 × 2	2.775(3)	–Li1	2.7748(9)	–Li2 × 2	2.733(1)
–Li2 × 2	2.835(3)	–Li4 × 2	2.797(1)	–Li5	2.788(2)
–Li1 × 2	2.938(2)	–Li3	2.853(2)	–Li3	2.817(2)
–Li1	3.092(5)	–Li2	2.891(2)	–Li5	2.954(2)
–Li2 × 4	3.2386(8)	–Li4	2.951(2)	–Li4	2.975(2)
–Li2	3.268(5)	–Li2	3.027(2)	–Li4	3.140(2)
		–Li4 × 2	3.188(2)	–Li1 × 2	3.2079(5)
		–Li3 × 2	3.224(1)	–Li5	3.231(3)
		–Li3	3.362(2)	–Li3 × 2	3.306(1)
		Li1–Al1 × 2	2.7748(9)		
		–Li2 × 2	2.840(2)		
		–Li5 × 4	2.847(2)		
		–Al2 × 4	3.2079(5)		
		–Li2 × 2	3.430(2)		
Li1–Li2 × 2	2.757(4)	Li2–Li3	2.716(3)	Li4–Li3	2.730(3)
–Al × 2	2.775(3)	–Al2 × 2	2.733(1)	–Li5	2.731(4)
–Li2 × 2	2.778(4)	–Li5 × 2	2.815(2)	–Al1 × 2	2.797(1)
–Al × 2	2.938(3)	–Li1	2.840(2)	–Li3 × 2	2.824(2)
–Al	3.092(5)	–Al1	2.891(2)	–Al1	2.951(2)
–Li1 × 4	3.239(1)	–Al1	3.027(2)	–Al2	2.975(2)
–Li2	3.408(6)	–Li4 × 2	3.193(2)	–Al2	3.140(2)
		–Li2	3.199(2)	–Li2 × 2	3.193(2)
		–Li5 × 2	3.361(3)	–Li4 × 2	3.203(3)
		–Li1	3.430(2)	–Li3	3.357(3)
Li2–Li1 × 2	2.757(4)	Li3–Li2	2.716(3)	Li5–Li4	2.731(40)
––Li1 × 2	2.778(4)	–Li4	2.730(3)	–Al2	2.788(2)
–Al × 2	2.853(3)	–Li3 × 2	2.794(2)	–Li5	2.814(4)
–Li2 × 2	2.860(6)	–Al2	2.817(2)	–Li2 × 2	2.815(2)
–Al × 4	3.239(1)	–Li4 × 2	2.824(2)	–Li1 × 2	2.847(2)
–Al	3.267(4)	–Al1	2.853(2)	–Al2	2.954(2)
–Li	3.408(6)	–Al1 × 2	3.224(1)	–Al1 × 2	3.188(2)
		–Al2 × 2	3.306(1)	–Al2	3.231(3)
		–Li4	3.357(3)	–Li2 × 2	3.361(3)
		–Al1	3.362(2)	–Li5	3.483(5)

HT phase decomposes at 330 °C to Li_3Al_2 and Li rich melt. Li_3Al_2 decomposes at 520 °C to LiAl (β phase) and Li rich melt. The employed reaction mixtures $Li_{91.5}Al_{8.5}$ and $Li_{96}Al_4$ cooled from 450 to 300 and 210 °C, respectively, would represent equilibria between HT-Li_9Al_4/melt and Li_9Al_4/melt, respectively.

The products obtained after isothermal centrifugation have a profoundly different appearance. The $Li_{96}Al_4$ mixture yielded large, mm-sized crystalline blocks with lamellae structured surfaces and dark, almost black luster. The product from the $Li_{91.5}Al_{8.5}$ mixture corresponded to needle shaped gray crystals with lengths up to 8 mm and thicknesses up to 1 mm. The X-ray powder patterns are shown in Fig. 3 and confirm that different products were obtained. The product of the $Li_{96}Al_4$ mixture corresponds to monoclinic Li_9Al_4. The lattice parameters extracted from the indexed pattern are $a=18.968(5)$ Å, $b=4.508(1)$ Å, $c=5.417(1)$ Å, $\beta=105.49(1)^\circ$. Some additional weak reflections in the powder pattern could not be identified. The $Li_{91.5}Al_{8.5}$ reaction produced a new phase. The diffraction peaks can be indexed with an orthorhombic cell ($a=4.6404(8)$ Å, $b=9.719(2)$ Å, $c=4.4764(8)$ Å). Remaining reflections stem from a small amount of monoclinic Li_9Al_4. The new phase was subsequently characterized as Li_2Al, crystallizing with the same structure as Li_2Ga and Li_2In [10,16]. The refinement of single crystal X-ray diffraction data showed that the Li atom positions in

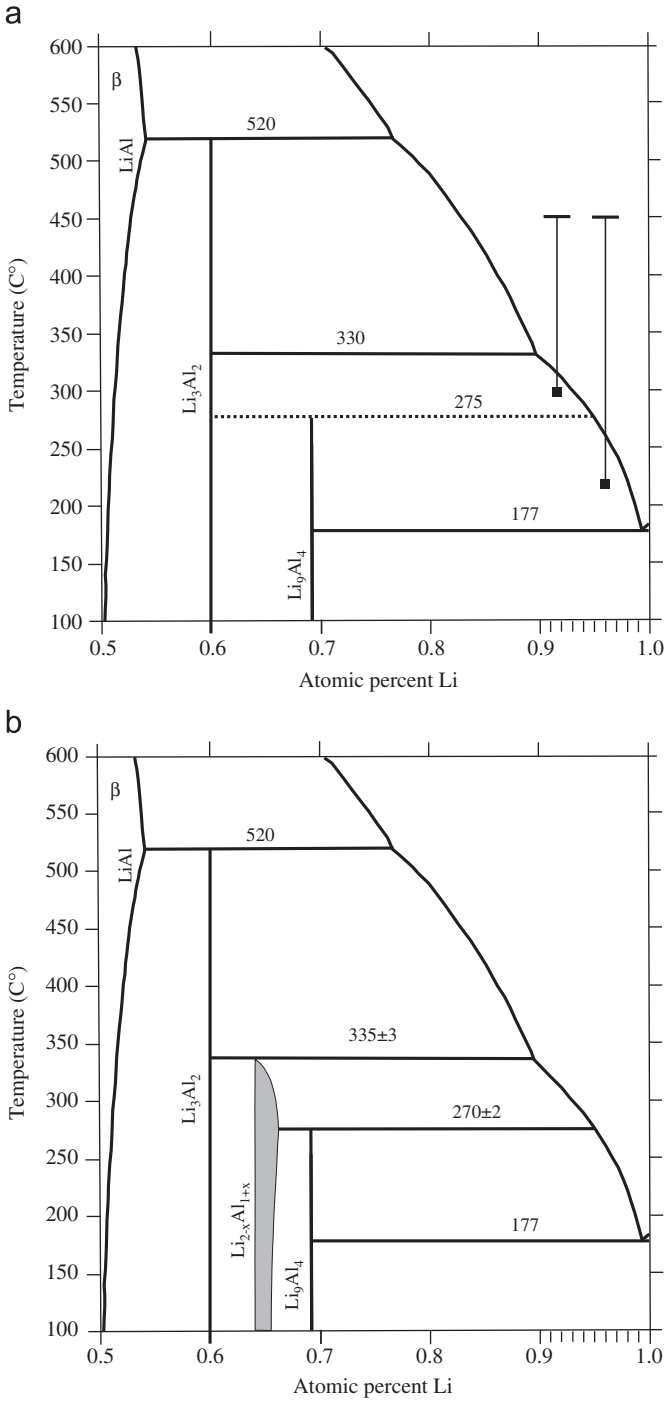

Fig. 2. (a) Li rich portion of the Li–Al phase diagram according to McAllister [6]. Reactions performed in this study are indicated by vertical lines. (b) Revised Li–Al phase diagram based on the findings of this study. The homogeneity range of $Li_{2-x}Al_{1+x}$ as sketched by the gray area has not been established.

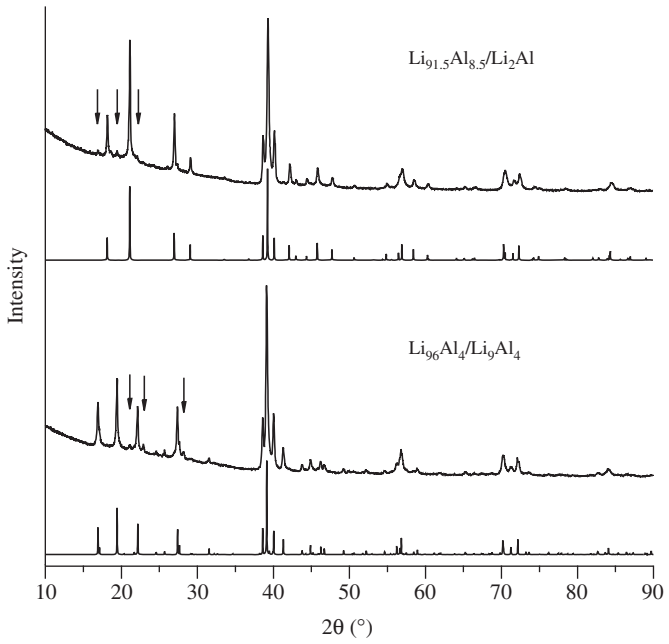

Fig. 3. Powder XRD pattern (Cu$K\alpha$) for the product of sample $Li_{91.5}Al_{8.5}$ (top) and $Li_{96}Al_4$ (bottom). The former corresponds to orthorhombic Li_2Al, the latter to monoclinic Li_9Al_4. Calculated patterns based on the refined structure from single crystal X-ray diffraction data are shown below the measured patterns. Arrows mark additional reflections. For $Li_{91.5}Al_{8.5}$ (Li_2Al) they correspond to Li_9Al_4, for $Li_{96}Al_4$ they are unidentified.

the Li_2Al structure were partially occupied with Al (refined total composition $Li_{1.92(1)}Al_{1.08(1)}$, 64 at% Li) which indicates a small homogeneity range, $Li_{2-x}Al_{1+x}$, for this phase.

The results for the thermal analysis of Li_9Al_4 and Li_2Al are depicted in Fig. 4. Each sample was first cycled between 50 and 300 °C three times and subsequently heated to 380 °C and cooled again. The DSC heating trace of Li_9Al_4 shows repeatedly a thermal event below 300 °C (Fig. 4a), with an onset at 270 ± 2 °C and the peak maximum at 274 ± 3 °C. The associated enthalpy is around 31 J/g. This event is attributed to peritectic decomposition of Li_9Al_4 into the new, more Al rich phase $Li_{2-x}Al_{1+x}$ and Li rich melt. This reaction is reversible upon cooling although the large hysteresis indicates a sluggish re-formation of Li_9Al_4. The peak maximum of the exothermic event is between 220 and 230 °C. When heating Li_9Al_4 to 380 °C, a second endothermic event occurs at 337/343 °C (T onset/T peak maximum). This event corresponds to the peritectic decomposition of $Li_{2-x}Al_{1+x}$ into Li_3Al_2 and Li rich melt. As expected, the DSC heating trace of $Li_{2-x}Al_{1+x}$ does not show a thermal event below 300 °C (Fig. 4b). The heating trace of the first cycle shows a weak and broad endothermic feature around 220 °C, which is obtained reproducibly for different samples and may relate to Li/Al ordering in this phase. The event at 334/341 °C (T onset/T peak maximum) in the 380 °C heating trace is the peritectic decomposition and matches the result from the Li_9Al_4 run. The enthalpy associated to the decomposition of $Li_{2-x}Al_{1+x}$ is around 93 J/g. The reaction is reversible upon cooling, with a small hysteresis. The onset and peak maximum temperatures are at 328 and 323 °C, respectively, in the cooling trace.

The new findings have been inserted in the original phase diagram which is shown revised in Fig. 2b. The discovery of the new phase Li_2Al ($Li_{2-x}Al_{1+x}$) resolves the mystery of the 275 °C isotherm. The occurrence of Li_2Al is probably not too surprising in light of the existence of isostructural Li_2Ga and Li_2In in the phase diagrams of the heavier congeners [10,16]. The crystal structures of orthorhombic Li_2Al and monoclinic Li_9Al_4 are closely related. During the course of this work we also reinvestigated the Li_9Al_4 structure. A comparison and discussion of the two structures is given in the following.

3.2. *Crystal structures of Li_2Al and Li_9Al_4*

The crystallographic data for both structures are compiled in Tables 1–3. Li_2Al crystallizes in the orthorhombic space group *Cmcm*. The structure consists of three atomic positions 4*c*, one for Al and two for Li (Li1 and Li2). Refinements of occupancies for the

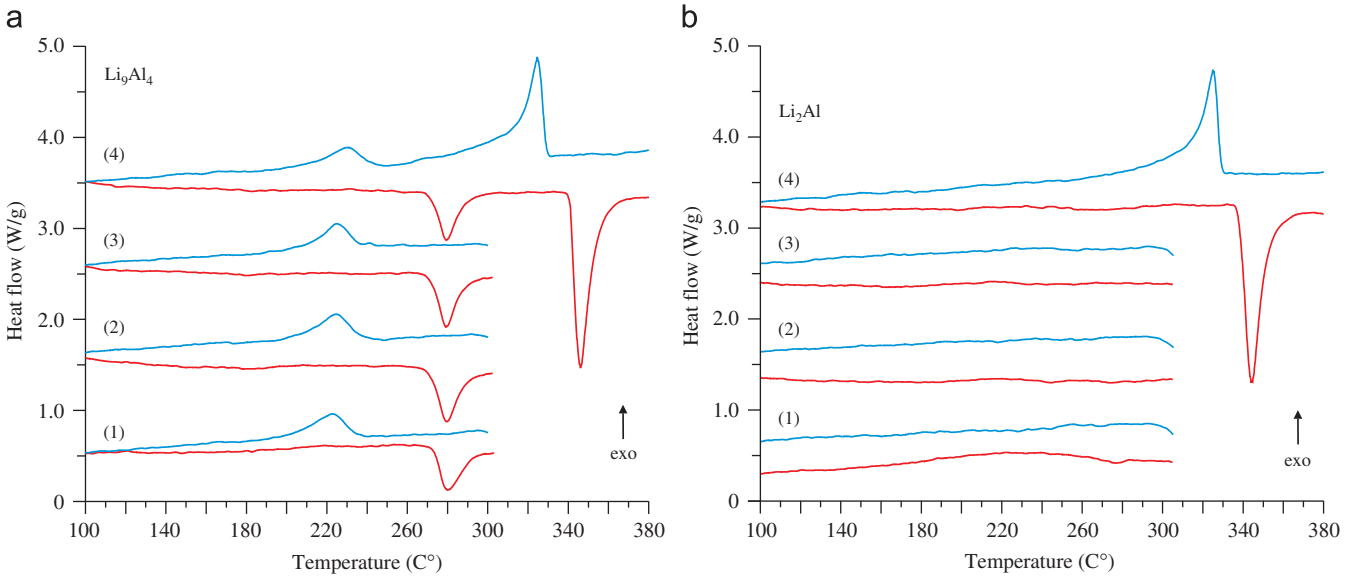

Fig. 4. DSC heating (red (lower) line) and cooling traces (blue (upper) line) for Li_9Al_4 (a) and Li_2Al (b). (1)–(3) indicate three consecutive heating/cooling cycles from 50 to 300 °C. (4) indicates a final heating/cooling cycle from 50 to 380 °C. The curves are offset arbitrarily for clarity. (For interpretation of the references to colour in this figure legend, the reader is referred to the web version of this article.)

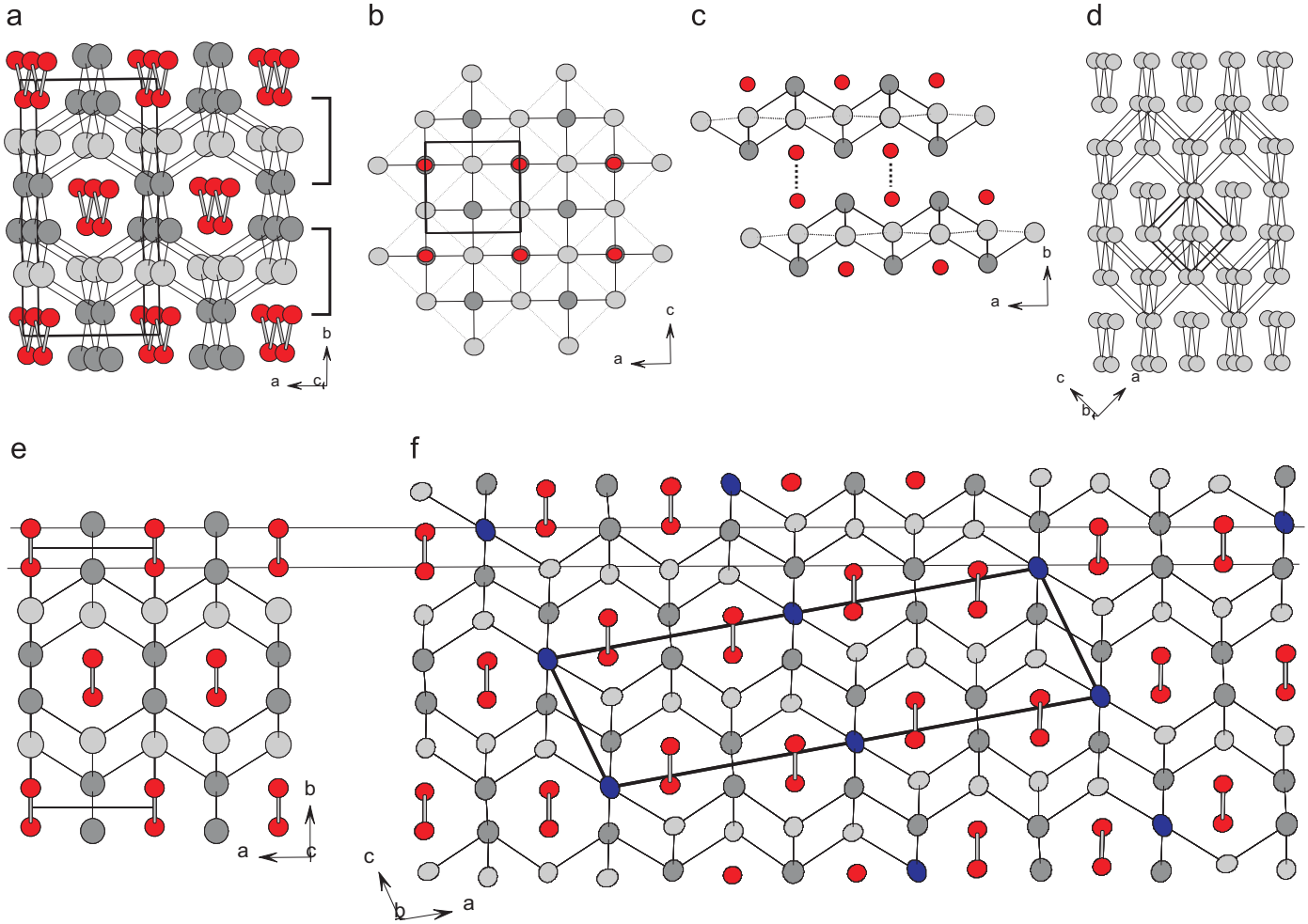

Fig. 5. (a) Crystal structure of orthorhombic Li_2Al. Light gray, dark gray, and red ellipsoids denote Li1 (equatorial), Li2 (apical), and Al atoms, respectively. Drawn bonds emphasize Li–Li and Al–Al distances smaller than 3 A. The unit cell is indicated by thick solid lines. (b) A layer of square pyramids formed by Li1 and Li2 atoms as building block of the Li_2Al structure. Al atoms complete the square pyramids to octahedra. The thickness of the layer is indicated by bars in (a). (c) Stacking of layers in the Li_2Al structure along the *b* direction. (d) The cubic bcc structure projected slightly off the [010] direction. Drawn bonds emphasize the topological relationship to the Li_2Al structure. (e) The Li_2Al structure projected along the [001] direction. (f) The monoclinic Li_9Al_4 structure projected normal to the *b* axis. The color code is the same as for Li_2Al structure (cf. (a)). Additional Li atoms are denoted by blue ellipsoids. Ellipsoids are drawn at the 90% probability level for all atoms. (For interpretation of the references to colour in this figure legend, the reader is referred to the web version of this article.)

Li sites, however, resulted in a significant lowering of the R1 index (from 0.033 to 0.025) when considering admixture with Al (4–5%). Nevertheless in the following we refer to these positions as Li atom positions. The more complex structure of Li_9Al_4 crystallizes monoclinic. Originally the structure was reported with $B2/m$ space group symmetry [12]. Here we present it in the conventional $C2/m$ setting. The unit cell of Li_9Al_4 has about twice the size of the Li_2Al one and contains two Al (Al1, Al2) and four Li (Li2-Li5) atomic positions 4*i*. Additionally there is a fifth Li site at 2a (Li1). In contrast with Li_2Al, refinements of site occupancies did not indicate the presence of significant Li/Al disorder. This supports the previous assignment of Li_9Al_4 as stoichiometric line compound [6].

The prominent feature of both structures is the arrangement of the Al atoms which form planar zigzag chains. These chains can be considered as polyanions. The Al–Al distance is 2.70 and 2.68 Å in Li_9Al_4 and Li_2Al, respectively. However, in the Li–Al system only the β phase LiAl with a diamond-like Al substructure formally corresponds to an electron precise Zintl phase. Here the Al–Al distance is 2.75 Å [8]. In Li_3Al_2 Al atoms form puckered hexagon layers with an Al–Al distance of 2.73 Å [9]. The Li rich phases, Li_3Al_2, Li_2Al and Li_9Al_4, are electron deficient with respect to the electronic requirement of a polyanionic substructure consisting of singly bonded Al atoms.

The structure of Li_2Al is shown in Fig. 5a. The Al zigzag chains run along the crystallographic *c* direction. The Li1 atoms (equatorial atoms) form an almost regular two-dimensional square net (Fig. 5b). The squares are alternately capped above and below by the Li2 atoms (apical atoms). In the resulting layer of square pyramids Li1 attains a quasi-tetrahedral coordination by four Li2 atoms. The Li1–Li2 distances are around 2.76 Å. The Al atoms complete Li1Li2 square pyramids to octahedra, and layers of edge condensed octahedra are now stacked along the *b* direction (Fig. 5c). The shift introduced by the *C*-centering arranges Al atoms and apical Li2 atoms into layer-connecting zigzag chains ($d_{Li2-Li2}=2.86$ Å).

A relationship between the Li_2Al (Li_2Ga) structure and the body centered cubic (bcc) structure is seen when focusing on the quasi-close-packed arrangement of atoms in the *bc* plane and its stacking along the *a* direction. This is shown in Fig. 5d. Quasi-close-packed planes of atoms in the bcc structure are perpendicular to the $\langle 110 \rangle$ directions. In Fig. 5d bonds were first drawn for 8+6 coordinated atoms and subsequently selectively removed to yield the connectivity of the Li_2Ga type structure. It should be noted that this relationship between bcc and Li_2Ga structure is of rather topological nature. The axial ratios of the orthorhombic unit cell of the Li_2Ga structure are $b/a \approx 2$ and $c/a \approx 1$, whereas the corresponding values for the bcc arrangement are $b/a=3$ and $c/a \approx 0.71$. However, the relationship is helpful for explaining the Li_9Al_4 structure. It is easily derived from the Li_2Al structure (Fig. 5e) by inserting into each quasi-close-packed layer an additional row of Li atoms after 12 regular rows of Li1, Li2 and Al atoms.

As for Li_2Al Al zigzag chains in the Li_9Al_4 structure are symmetry equivalent but now composed of two different kinds of Al atoms. Likewise there are two kinds of apical (Li2 and Li4) and equatorial Li atoms (Li3 and Li5), respectively. The inserted Li atoms (Li1) have the connectivity of apical atoms. Interatomic distances for nearest neighbor pairs Li–Li and Li–Al are very similar to Li_2Al (Table 3).

4. Conclusions

A new phase was discovered in the binary system Li–Al. Li_2Al is isostructural to orthorhombic Li_2Ga and Li_2In and possesses most likely a small homogeneity range $Li_{2-x}Al_{1+x}$. Refinement of site occupancies from single crystal X-ray diffraction data yielded a composition $x \approx 0.08$. Li_2Al is formed peritectically by reaction of Li_3Al_2 with Li rich melt at 335 ± 2 °C. It is also the product of the peritectic decomposition of Li_9Al_4 at 270 ± 2 °C. Li_2Al and monoclinic Li_9Al_4 have closely related structures. Al atoms are arranged into planar zigzag chains, which are encapsulated in channels formed by up and down facing square pyramids of Li atoms.

Acknowledgments

This research has been supported by the National Science Foundation through Grants DMR-0638826 and CHE-0742006.

Appendix A. Supplementary material

Supplementary data associated with this article can be found in the online version at doi:10.1016/j.jssc.2010.08.029.

References

[1] T.O. Brun, J.D. Jorgensen, M. Misawa, F.J. Rotela, S. Susman, J. Electrochem. Soc. 129 (1982) 2509.
[2] K.M. Myles, F.C. Mrazek, J.A. Smaga, J.L. Seetle, 1976. Advanced battery research and design. In: US ERDA Report ANL-76-8. Proceedings of the Symposium and Workshop, Argonne National Laboratory, pp. B50–B73.
[3] E. Schürmann, H.-J. Voss, Giessereiforschung 33 (1981) 33.
[4] R.J. Pulham, P. Hubberstey, P. Hemptenmacher, J. Phase Equilibria 15 (1994) 587.
[5] N. Saunders, Z. Metallkd. 80 (1989) 894.
[6] A.J. McAllister, Bull. Alloy Phase Diagrams 3 (1982) 177.
[7] B. Hallstedt, O. Kim, Int. J. Mater. Res. 98 (2007) 961.
[8] K. Kuriyama, N. Masaki, Acta Crystallogr. B 31 (1975) 1793.
[9] K.-F. Tebbe, H.G. von Schnering, B. Rüter, G. Rabeneck, Z. Naturforsch. B 28 (1973) 600.
[10] W. Müller, J. Stöhr, Z. Naturforsch. B 32 (1977) 631.
[11] J. Stöhr, H. Schäfer, Z. Naturforsch. B 34 (1979) 653.
[12] D.A. Hansen, J.F. Smith, Acta Crystallogr. B 24 (1968) 913.
[13] M. Boström, S. Hovmöller, J. Solid State Chem. 153 (2000) 398.
[14] G.M. Sheldrick, in: SADABS Version 2.10, University of Göttingen, Germany, 2003.
[15] G.M. Sheldrick, in: SHELXS97 and SHELXL97, University of Göttingen, Germany, 1997.
[16] J. Stöhr, W. Müller, H. Schäfer, Z. Naturforsch. B 33 (1978) 1434.